

Keywords: frontal collision; airbag; DP-type AHSS steel

**Dominik GALDYNski^{1*}, Karol F. ABRAMEK², Maciej LISOWSKI³,
Wawrzyniec GOLEBIEWSKI⁴, Tomasz OSIPOWICZ⁵**

HEURISTIC MODEL FOR ASSESSING DISRUPTIONS IN THE SYNCHRONIZATION OF AIRBAG DEPLOYMENT WITH THE DRIVER'S BODY DURING A COLLISION, BASED ON REPAIRED LONGITUDINAL BEAMS

Summary. The article presents a heuristic model used to evaluate the level of disorder in the synchronization of airbag operation with a moving phantom head during a frontal collision caused by a change in the longitudinal stiffness. The article describes three areas of research. The first presents the results of the strength tests of longitudinal models: reference and welded joint. Based on these, the relative stiffness decrease coefficient (SDC) of the longitudinal was determined. The second presents an analytical model of the airbag activation algorithm and the impact of SDC on its operation. The third determined the contact time of the phantom head with the airbag, taking into account the SDC. Based on the selected case study, a spatiotemporal analysis was conducted, indicating the level of disorder in the synchronization of the airbag with the moving phantom head due to the change in longitudinal stiffness.

1. INTRODUCTION

The airbag is the last significant step in the concept of passenger vehicle safety and complements the seat belts. Despite its obvious benefits, it can also generate dangers. The first arises from too high an inflation pressure [22]. The second comes from an incorrect passenger position [23]. The third is from a change in the stiffness of the vehicle body [3]. The article presents a study of the last case. The activation of the airbag is based on the diagnosis of the deceleration signal recorded by the accelerometer located in the control module [11]. The deceleration depends on the collision speed and the stiffness of the vehicle body [5].

Efforts by vehicle manufacturers to reduce exhaust toxicity by reducing the weight of the body or improving passenger safety are achieved through the use of high-strength steels such as Advanced High-Strength Steel (AHSS). Maintaining the original stiffness of this steel during post-collision repairs is a key technological problem. Intervention in the structure of a car body made of AHSS steel using Gas Metal Arc Welding (GMAW) methods with M21 gas shield (82% Ar and 18% CO₂) and G3Si1, AWS ER70S-6 (Rm 560 [MPa]) filler material causes a decrease in its original strength

¹ West Pomeranian University of Technology in Szczecin, Department of Automotive Engineering; Piastow av. 19, 70-310 Szczecin, Poland; e-mail: dgaldynski@zut.edu.pl; <https://orcid.org/0000-0003-3232-2656>

² West Pomeranian University of Technology in Szczecin, Department of Automotive Engineering; Piastow av. 19, 70-310 Szczecin, Poland; e-mail: kabramek@zut.edu.pl; <https://orcid.org/0000-0001-9704-5253>

³ West Pomeranian University of Technology in Szczecin, Department of Automotive Engineering; Piastow av. 19, 70-310 Szczecin, Poland; e-mail: mlisowski@zut.edu.pl; <https://orcid.org/0000-0002-0708-7132>

⁴ West Pomeranian University of Technology in Szczecin, Department of Automotive Engineering; Piastow av. 19, 70-310 Szczecin, Poland; e-mail: wgolebiewski@zut.edu.pl; <https://orcid.org/0000-0002-3691-8636>

⁵ West Pomeranian University of Technology in Szczecin, Department of Automotive Engineering; Piastow av. 19, 70-310 Szczecin, Poland; e-mail: tosipowicz@zut.edu.pl; <https://orcid.org/0000-0002-3321-7754>

* Corresponding author. E-mail: dgaldynski@zut.edu.pl

properties. Interest in the negative impact of welding processes on the properties of AHSS steel has intensified with the use of steels with strengths above 600 [MPa] for car body construction. This value is the minimum threshold for the noticeable influence of the welding process on the strength of such a joint [20].

In the research published in [13], it was noticed that welded connections of AHSS steel may exhibit lower mechanical properties compared to native materials because the amount of heat input during welding significantly alters the original microstructure in the weld and HAZ (heat-affected zone), showing lower tensile strength by 20 to 40% than the native material. In article [19], the authors examined the hardness distribution of such a connection. The average hardness in the HAZ was 75% of the hardness of the native material. The hardness of such connections was also studied by the authors in article [20], which indicated that the decrease in hardness in the HAZ is particularly significant in steels above 600 MPa. Other researchers in article (9) pointed out a linear relationship between the hardness and tensile strength of high-strength steel in the range of 450-2350 MPa.

The cited studies indicate that the impact of the GMAW welding process significantly reduces the load-bearing capacity and stiffness of elements made of AHSS steel. Such a change in stiffness, for example in a longitudinal member of a vehicle body made of AHSS steel, acquired during reconstruction after an accident, will determine the course of vehicle deceleration in the event of a subsequent collision. This view was confirmed in article [3], in which the authors present research results showing that the process of partial replacement of the front body longitudinal member implies a 30% decrease in its strength compared to an unrepaired longitudinal member. In a subsequent article [4], the same authors compare the results of dynamic tests of an energy-absorbing model (longitudinal member) with a numerical model for FEA analysis and a real object (vehicle). They demonstrate the possibility of using the analogy of a longitudinal member for the crash tests of the entire vehicle, of course, at the initial stage of deformation, where it plays a dominant role in absorbing the impact energy.

2. STRUCTURAL TESTING

Despite the extensive literature mentioned in the introduction, structural testing on longitudinal member models was repeated. The geometrical dimensions of the models remained consistent with those used by the authors [10] for verifying the obtained results. The testing was conducted for a simple stress state of a compressed model. The models were made of AHSS steel type DP 1000. The reference structures MPr(i) and the welded joint with a ground weld face MPr(i)-weld/grind were subjected to testing. The connection method was replicated according to the technology of partial replacement of a car body longitudinal member [7]. The obtained results, which were subjected to statistical analysis, are presented in Fig. 1 and Table 1.

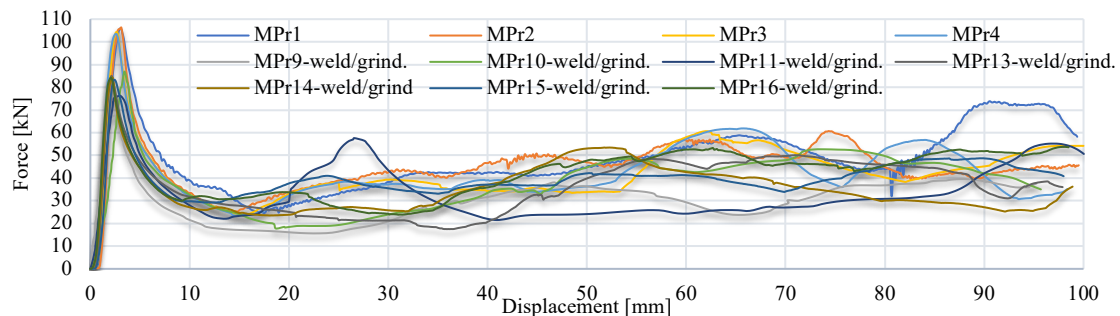


Fig. 1. Compression force characteristic as a function of the displacement of the machine piston, from empirical tests of the energy-absorbing structure of a one-legged profile at an angle of 0 degrees to the longitudinal axis of the system, profiles without welded joint MPr(i), and with welded joint with a ground joint face MPr(i)-weld/grind

A characteristic feature of this type of destruction process during the longitudinal beam compression is the appearance of a subsequent fold only after the previous one is closed. Therefore, the energy absorption process during the deformation of the longitudinal beam can be considered separately for each successive fold [1]. The size of the fold is closely related to the geometric parameters of the longitudinal beam and depends on the narrowest wall width of the cross-section [1, 17]. A change in shape occurs at the weakest point of the cross-section [10]. Therefore, a welded joint with a ground weld face will cause the first fold to appear at the location of such a joint. The length over which the stiffness change of the longitudinal beam will cause a decrease in the kinetic energy absorption during the collision corresponds to the section to close the first fold of the longitudinal beam. The further course of energy absorption in the process of compressed folds will be identical to the case without such changes.

Table 1

Statistical analysis of the percentage decrease in the values of parameters E_c , P_{max} , for specimens with welded joints with ground weld bead, relative to the arithmetic mean value of parameters E_c , P_{max} , for reference specimens

Samples with ground joint	decrease in value E_c [J]	decrease in value P_{max} [kN]
MPr9-weld/grind	32.92%	35.40%
MPr10-weld/grind	45.88%	17.24%
MPr11-weld/grind	26.03%	27.41%
MPr13-weld/grind	21.33%	40.20%
MPr14-weld/grind	30.05%	19.15%
MPr15-weld/grind	32.00%	19.54%
MPr16-weld/grind	23.41%	20.67%
Arithmetic average	30.23%	25.40%

The amount of absorbed energy of deformations. [10] $E_c = \int_0^{\delta_k} F(\delta) d\delta = F_S \delta_K [J]$ (1)

The maximum force during compression. [10] $P_{max} = \max[F(\delta)], \delta \in (0, \delta_k), [N]$ (2)

The results of the conducted research showed a 30% (SDC) decrease in energy absorption during deformation and a 25% decrease in the maximum force required to initiate plastic deformation of the compressed structure for models with the MPr(i)-weld/grind joint.

3. THE INFLUENCE OF ANTERIOR TIBIAL STIFFNESS CHANGE ON THE ACTIVATION TIME OF AIRBAG

For example, based on the NHTSA FMVSS No. 208 crash test: frontal collision, Honda Civic, collision speed of 23, 32, 40, 48, 56 km/h into a non-deformable obstacle with a driver dummy [14], further research results will be presented. For the same vehicle collision speed, a logical consequence of changing the longitudinal stiffness of the structure, which is used to measure the deceleration by the airbag control module, is a change in activation time, and therefore the reference state of the airbag. Based on the mathematical models used in airbag activation algorithms [11], an energy-based model was utilized for the analysis.

$$E_c = \frac{m^*(v_a^2 - v_b^2)}{2} \quad (3)$$

where:

v_1^2 – the instantaneous collision speed at the beginning of the signal measurement (e.g. after the vehicle exceeds 9.81 [m/s²] deceleration) [11],

v_2^2 - the instantaneous collision velocity at the end of the signal measurement (e.g., after 5 [ms] from the moment of the vehicle exceeding 9.81 [m/s²] deceleration) [11],

m – the actual weight of the vehicle.

The energy-based parameter selection resulted from the convergence with the parameter generated based on the conducted experiments. After determining the variable of 30% SDC, it was introduced into the developed model. Figure 2 presents its graphical representation. Based on this model and the value of E_c taking into account the determined decrease in energy absorption under deformation (Fig. 2, green curve), a new corrective time for the reference state of the airbag was determined (Fig. 2, dashed curves).

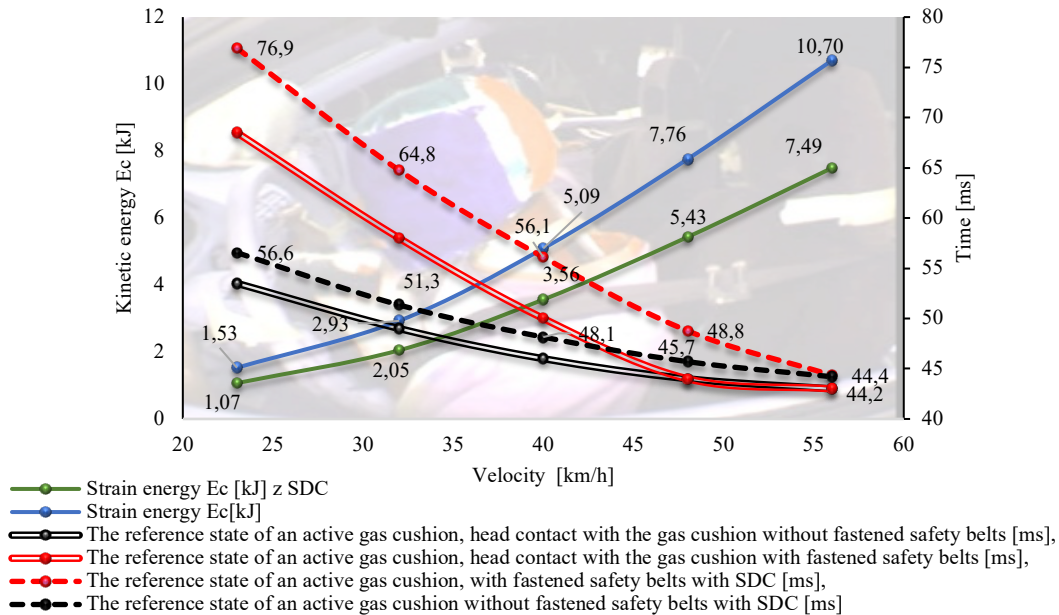


Fig. 2. Energy parameters E_c and newly generated reference airbag activation times for crash tests with a belted and unbelted phantom driver as a function of collision velocity for the Honda Civic vehicle

The original stiffness of the vehicle on the signal deceleration diagnosis section for the measured energy E_c (blue curve) resulted in a 30% decrease in E_c after considering SDC (green curve). This value, interpreted based on the original relationship in the airbag control module settings, corresponds to lower collision speeds. Such a change will cause the reference state of the airbag to be reached later (dashed lines) for a given collision speed than originally predicted (double lines). Lower speed generates less energy, which requires a later activation of the airbag, equivalent to a later reference state time. Because the pressure curve in the airbag has a phase character, contact between the head and the airbag must occur when the pressure inside it reaches its maximum, but not later [16]. It is this point in the pressure phase curve that allows for optimal head deceleration.

Increased susceptibility of the bodywork to deformation due to SDC of the longitudinal members will result not only in a later reference time for the gas cushion, as determined in this chapter, but also in a relative elongation of the distance and, consequently, the time required for the phantom's head to reach the gas cushion. To determine whether the original synchronization of these times will be maintained as it is for factory conditions (Fig. 2, double curves), the time at which this correct contact should occur must be determined, taking into account SDC. After determining this time, it should be compared with the time determined for the reference state of the gas cushion (Fig. 2, dashed curves). During the design of the SRS system at the vehicle construction stage, the determined time for the correct contact of the gas cushion with the driver's head is used to calibrate the activation of the gas cushion so that its reference state is achieved at this determined time.

4. IMPACT OF CHANGE IN LONGITUDINAL BEAM STIFFNESS ON CONTACT TIME BETWEEN PHANTOM HEAD AND AIRBAG

The correct time of contact between the driver's head and the airbag is determined based on the "13-30" principle [2,8]. The graphical presentation of this principle is shown in Figure 3. Based on the deceleration curve recorded during the crash test, the trajectory of the phantom head and the vehicle within the steering wheel are determined. Taking into account the normalized distribution of the phantom head and the design parameters of the vehicle, the time in which the airbag should reach its full functionality, i.e., the reference state, to properly take over the driver's head during a collision, is determined for a given distance, e.g., 13 cm. Similarly, times for other tested collision speeds are determined.

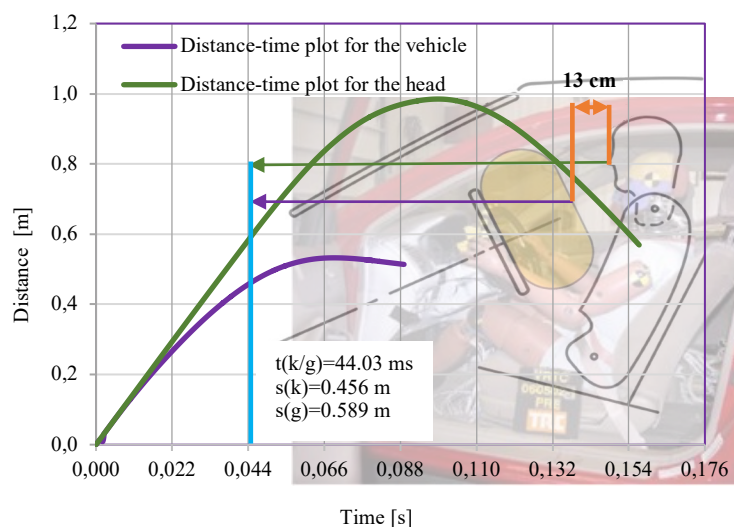


Fig. 3. Graph of distance as a function of time for the driver's head and vehicle with the indicated correct contact time for the FMVSS208 crash test at a speed of 48 km/h [14]. *The labels shown in Figure 3 are explained in Table 2

During a vehicle's impact with an obstacle, the head and steering wheel, in which the airbag is mounted, have approximately the same direction and rotation, but variable velocity relative to each other. Due to the fact that the steering wheel is decelerated, and the phantom's head does not come into contact with the airbag, the distance between them is reduced (in the case of a crash test with a phantom without a seatbelt [14]). To determine the correct contact between the driver's head and the airbag taking into account SDC, a heuristic model was developed to conduct spatiotemporal analysis

The analysis conducted for the phantom head and the vehicle will be based on the coordinates of the deceleration measurement established during the crash test. To carry out this task, the parameters of the distance and time for the phantom head were determined first. Based on the reports from the crash test [14], the exact time at which the driver's head makes contact with the airbag was determined to be 44.03 [ms]. Using the relationship from equation 4, the length of the traveled distance of the phantom head $s(g)$ to the contact with the airbag was determined:

$$VI(k/g) = \frac{s(g)}{t(k/g)} \quad (4)$$

where:

$VI(k/g)=13,38$ [m/s] - velocity of the phantom head at the contact with the airbag,

$t(k/g)=44,03$ [ms] time of contact of airbag with the head,

$s(g)=0,589$ [m] - the trajectory of the head towards contact with the airbag

Next, based on the recorded deceleration profile of the vehicle during the crash test [14], its kinetic energy at the time of the real collision was determined. This parameter served as a basic unit for further calculations, which were divided into three stages. The first stage assumes the extraction of an area from the deceleration profile in which the decrease in energy absorption due to deformation (SDC) will be

taken into account. It was assumed that the length of the SDC influence on the vehicle body would be limited to the section until the closure of the first folded longitudinal member. Assuming that the further absorption of the collision will be identical to the case without SDC, new values of the vehicle's kinetic energy were determined for the end of this area, i.e., stage 1, and the time in which it will be covered (Fig. 4, blue indicator).

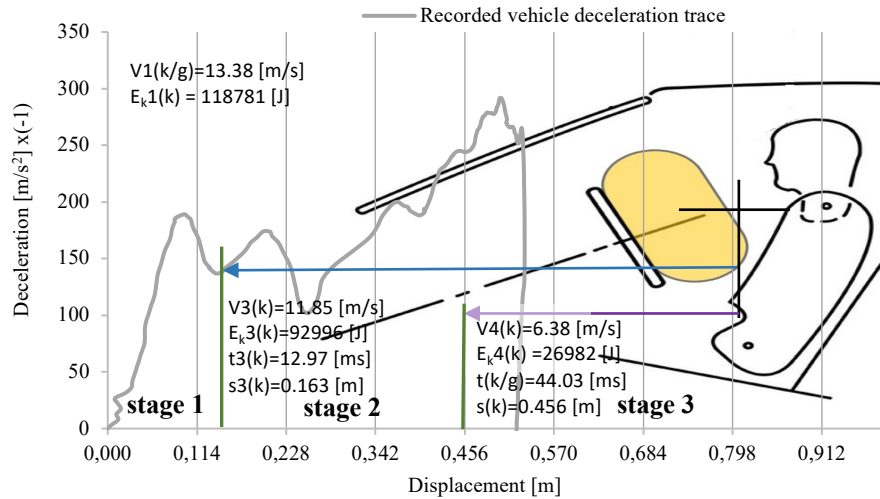


Fig. 4. The diagram of the steering wheel layout with an airbag and marked characteristic areas for spatiotemporal analysis is shown on the graph of the Honda Civic vehicle deceleration in the FMVSS 208 crash test at a collision speed of 48 km/h [14]

*the labels shown in Fig. 4 are explained in Table 2.

In the second stage, an area was extracted from the vehicle deceleration curve, from the end of stage 1 to the point where the phantom head contacted the airbag at the factory designated location. For this stage, a probabilistic model was developed by relating the parameters of distance and time for the phantom head contact with the airbag in stage 2 to the measured kinetic energy of the vehicle at the end of stage 1. The graphical representation of this model for the crash test results at speeds of 23, 32, 40, 48, and 56 [km/h] is shown in Fig. 5. The distance and time plotted on the y and x-axes, respectively, represent quantities measured in stage 2 and do not include the distance and time from stage 1.

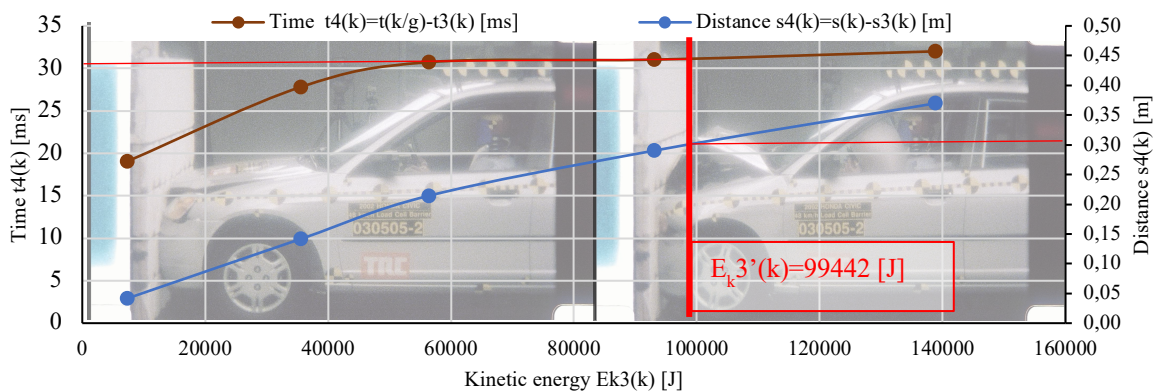


Fig. 5. Linear approximation plots of the coordinates of the independent variable parameter, vehicle kinetic energy $E_{k3}(k)$, for stage 1, and the dependent variable values, time $t_4(k)$ and distance $s_4(k)$, for stage 2, determined based on crash tests at speeds of 23, 32, 40, 48, and 56 [km/h] [14]

Thus, a probabilistic model of the correlation between the time and distance required to complete the second stage as a function of the kinetic energy of the vehicle at the end of the first stage was developed. A new variable was introduced into the model, which took into account the SDC for the end of the first stage, i.e. $E_{k3}'(k) = 99442$ [J]. Its higher value than the original one, for the assumed crash test speed of

48 km/h, results from the smaller amount of energy absorbed by the vehicle in the first stage due to SDC. Based on this, the model generated a forecast for the second stage, in which the vehicle covered a longer distance $s4'(k)$ in only slightly longer time $t4'(k)$.

In this way, new coordinates on the y-axis for distance $s4'(k)$ and time $t4'(k)$ were determined for the new independent variable $Ek3'(k)$ (Fig. 5).

$$s4'(k)=0302 \text{ [m]}, t4'(k)=31,18 \text{ [ms]}$$

The newly determined position and time at which the steering wheel with the airbag was found highlight the differences compared to its original position, where the distance $s4(k)$ and time $t4(k)$ were:

$$s4(k) = 0,2901 \text{ [m]}, t4(k) = 31,06 \text{ [ms]}$$

Thus, the position of the airbag relative to the phantom's head was determined in the new configuration. For further analysis, it was necessary to determine the vehicle velocity at the end of stage 2, taking into account SDC and without. It was calculated using the formula:

$$Vsr[s(k)] = s4(k)/t4(k) = 9,34 \text{ [m/s]} \tag{5}$$

$$Vsr'[s'(k)] = s4'(k)/t4'(k) = 9,69 \text{ [m/s]} \tag{6}$$

$$Vsr[s(k)] = \frac{V3(k)-V4(k)}{2} \tag{7}$$

$$Vsr'[s'(k)] = \frac{V3'(k)-V4'(k)}{2} \tag{8}$$

$$V4(k) = 2 * Vsr[s(k)] - V3(k) = 6,83 \text{ [m/s]} \tag{9}$$

$$V4'(k) = 2 * Vsr'[s'(k)] - V3'(k) = 7,12 \text{ [m/s]} \tag{10}$$

In the third stage, the new coordinates of the steering wheel with the airbag were linked to the coordinates of the head position through appropriate equations of motion. The time it takes for them to come into contact was determined, taking into account the calculated differences in their displacements.

For the time, it was denoted by the symbol $tr(k/g)$:

$$t_r(k/g) = t'(k) - t(k/g) = 0,09 \text{ [ms]} \tag{11}$$

For the distance, it was denoted by the symbol $sr(k/g)$:

$$s_r(k/g) = s'(k) - s(k) = 0,012 \text{ [m]} \tag{12}$$

The graphical presentation of the results is shown in Fig. 6.

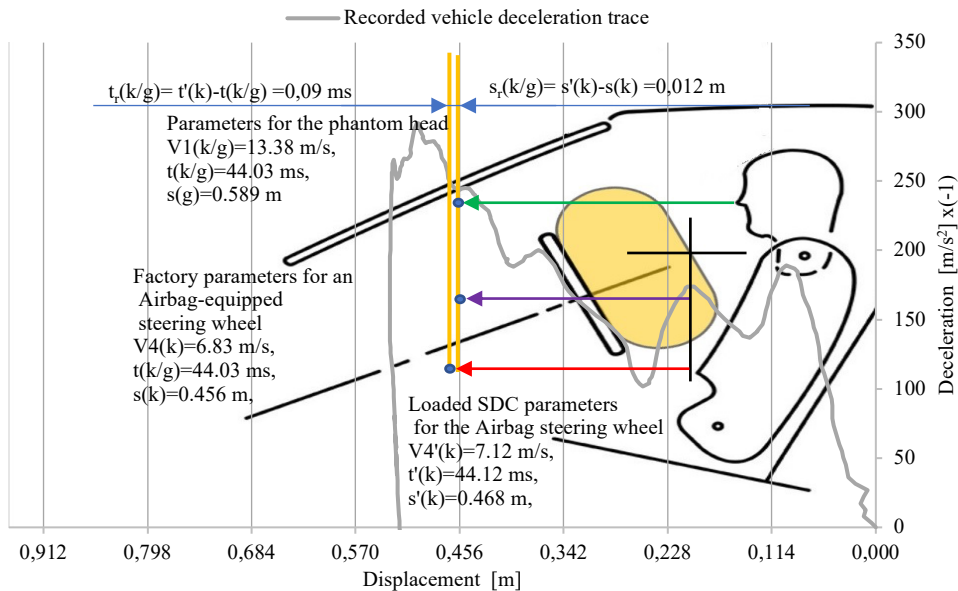


Fig. 6. Diagram of the position of the steering wheel with airbag relative to the phantom's head in the new configuration on the graph of the Honda Civic vehicle deceleration curve for a collision speed of 48 km/h, FMVSS Nr 208 crash test, with the phantom unrestrained by seat belts [14]

Based on the newly determined coordinates of the vehicle's steering wheel position, and thus the airbag's position, its path was described by an equation s_{ox} :

$$s_{ox} = V4'(k) * t_{x0} + \frac{a * t_{x0}^2}{2} \quad (13)$$

where:

t_{x0} – the time it takes for the head to come into contact with the airbag [s],

a – the deceleration at which the steering wheel/vehicle moves [m/s²].

Similarly, the path of the phantom's head was described by an equation, taking into account the displacement $s_r(k/g)$ and the time $t_r(k/g)$:

$$s_{ox} + s_r(k/g) = V1(k/g) * [t_{x0} + t_r(k/g)] \quad (14)$$

The equations formulated in this way were expressed as functions and equated to each other:

$$V1(k/g) * [t_{x0} + t_r(k/g)] - s_r(k/g) = V4'(k) * t_{x0} + \frac{a * t_{x0}^2}{2} \quad (15)$$

After rearrangement:

$$a * \frac{t_{x0}^2}{2} - V1(k/g) * t_{x0} + V4'(k) * t_{x0} - V1(k/g) * t_r(k/g) + s_r(k/g) = 0 \quad (16)$$

Before determining the zero point of this equation, which determines the time t_{x0} at which the two components meet, it was necessary to determine the value of the deceleration parameter a . Due to the variability of this parameter over time, the following methodology was proposed to determine its value. Equation 19 was transformed into a first-degree polynomial. Such an equation will determine the time at which the two components subject to the first principle of dynamics will meet. Then, the arithmetic mean of the instantaneous deceleration over the determined length of time will be taken into account

$$-V1(k/g) * t_{x0} + V4'(k) * t_{x0} - V1(k/g) * t_r(k/g) + s_r(k/g) = 0 \quad (17)$$

Due to the narrow time interval of 1.71 [ms], the determined value of deceleration based on it will be reliable. Therefore, the average value of deceleration will be:

$$a = (-244) \text{ [m/s}^2\text{]}$$

By substituting the established parameters into equation 19, the following was obtained:

$$122 t_{x0}^2 + 6,27 t_{x0} - 0,0107 = 0 \quad (18)$$

And the sought zero of this function was determined:

$$t_{x0} = \frac{-b \pm \sqrt{\Delta}}{2a} = 0,00166 \text{ [s]} \approx 1,66 \text{ [ms]} \quad (19)$$

The total time of displacement for the phantom head and the vehicle steering wheel with airbag until their contact at a speed of 48 km/h, denoted by the symbol $t_{cp-bp}(g/k)$, is determined from the equation for the phantom head and the vehicle steering wheel:

$$t_{cp-bp}(k/g) = t(k/g) + (t_{x0} + t_r(k/g)) = t'(k) + (t_{x0}) = 45,78 \text{ [ms]} \quad (20)$$

This means that due to the change in vehicle stiffness in stage 1, the time in which the head of the dummy should come into contact with the airbag according to the "13-30" rule increased by 1.75 [ms] compared to the originally determined time $t(k/g) = 44.03$ [ms]. Similar analyses were conducted for other crash test speeds. The parameters used in these calculations are presented in Table 2.

Similarly, to the crash test with a phantom without seat belts, an analysis was conducted for the crash test with a phantom wearing seat belts. The equation of the phantom's head movement was expanded by a deceleration term related to the active seat belts, determined analogously to the vehicle in equation 20. The results of the calculation analysis for evaluating disturbances in the synchronization of the airbag operation with the driver's body during the collision are presented in Table 3. They determine new $t_{cp-zp}(k/g)$ i $t_{cp-bp}(k/g)$ times at which the phantom's head should make contact with the airbag according to the "13-30" rule to maintain their proper synchronization.

In the first and second rows of Table 4, the modeling results for the crash test with the phantom restrained by seat belts are presented. They indicate the $t_{cp-zp}(k/g)$ contact time required to maintain synchronization between the moving head of the phantom and the airbag. In the third and fourth rows of Table 4, the modeling results for the crash test with the phantom unrestrained by seat belts ($t_{cp-bp}(k/g)$) are presented. The obtained times are compared with the reference airbag deployment times $t(k/g)$ from SDC, determined in the previous section. The graphical presentation of the obtained results is shown in Fig. 7.

Table 2

Comparison of characteristic parameters for the analysis of
a crash test with a dummy without seat belts [14]

	56km/h	48km/h	40km/h	32km/h	23km/h
Actual collision speed, $V1(k/g)$ [km/h]	56.5	48.2	40.2	31.7	22.9
Actual collision speed, $V1(k/g)$ [m/s]	15.69	13.38	11.17	8.81	6.36
Vehicle kinetic energy $E_k1(k)$ [J]	164938	118603	77981	58600	30539
Distance to first P_{max} $s2(k)$ [m]	0.101	0.098	0.094	0.098	0.105
Time to first P_{max} $t2(k)$ [ms]	6.5	7.4	8.6	12.3	18.8
The first stage segment $s3(k)$ [m]	0.166	0.163	0.159	0.163	0.170
Collision time at the end of the 1 stage $t3(k)$ [ms]	11.0	12.97	15.27	21.21	34.47
The speed of the steering wheel/veh. $V3(k)$ ** [m/s]	14.4	11.85	9.5	6.9	3.1
Vehicle kinetic energy $E_k3(k)$ ** [J]	138805	92996	56321	35489	7234
The distance of the steering wheel to the contact of the airbag with the head $s(k)$ [m]	0.537	0.456	0.375	0.304	0.212
E_k of the vehicle at the moment of contact between the airbag and the head $E_k4(k)$ [J]	40067	26982	10886	9115	1323
Time of contact of airbag with the head $t(k/g)$ [ms]	43.04	44.03	46.04	49.03	53.47

** - At the end of the first stage

Table 3

Reference state times of the airbag $t(k/g)$ with SDC and Time of contact of airbag with the head to the "13-30" principle with SDC with seat belts $t_{cp-zp}(k/g)$ and without seat belts $t_{cp-bp}(k/g)$, for collision speeds of 23, 32, 40, 48, 56 [km/h]

	23 [km/h]	32 [km/h]	40 [km/h]	48 [km/h]	56 [km/h]
time $t_{cp-zp}(k/g)$ [ms]	72.9	61.0	51.8	45.8	44.4
time $t(k/g)$ [ms] z SDC	76.9	64.8	56.1	48.8	44.4
time $t_{cp-bp}(k/g)$ [ms]	57.8	52.8	48.0	45.8	44.4
time $t(k/g)$ [ms] z SDC	56.6	51.3	48.2	45.7	44,2

The plotted curves in the chart (Fig. 7) represent the time of the reference state of the airbag (dashed curve in red and black) and the time of contact between the airbag and the phantom head for their proper synchronization (solid curve in red and black). As can be observed, for the case of a crash test with a phantom restrained by safety belts, these times differ significantly. This is because, despite the later contact time between the airbag and the phantom head caused by SDC, this change did not allow for the deceleration in activation and, consequently, the reference state of the airbag to be compensated. The absence of the airbag ready to receive the driver's head in the appropriate position will cause the head to intrude into the space that the airbag will only occupy later. Such asynchrony results in the driver's head meeting the airbag during its inflation.

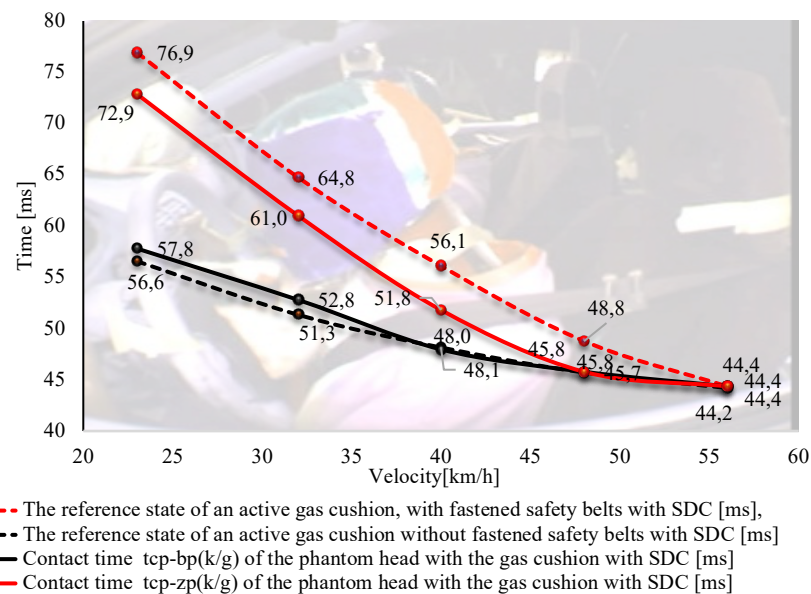


Fig. 7. Comparison of reference times of the gas cushion state with the times of contact between the phantom head and the gas cushion, loaded with SDC, as a function of collision speed

5. CONCLUSIONS

Based on the conducted research, the following conclusions have been formulated:

1. In the adopted models of longitudinal rails made of DP 1000 steel during compression strength tests, a decrease in deformation energy absorption by 30% and a decrease in the maximum force required to initiate plastic deformation of the compressed structure by 25% were observed for models with a welded joint made by the GMAW method.
2. This decrease is closely related to the change in activation time of the airbag and its interaction with the moving driver's head during a frontal collision.
3. The results of the spatiotemporal analysis indicated significant disturbances in the synchronization of the airbag with the moving phantom head.
4. The conducted modeling showed that in the extreme case, the moving phantom head reached the point of contact with the airbag 4.3 ms before it reached its full functionality.

The developed model allows for taking into account other cases beyond the described influence of the welding process. The change in the stiffness of the body can be influenced by the quality of the replacement parts used, such as longitudinal rails or bumper absorbers.

References

1. Abramowicz, W. Thin-walled structures as impact energy absorbers. In: *International Conference on Thin-Walled Structures Location*. 2003. Vol. 41 No. 2. P. 91-107.
2. Ching-Yao Ch. *Fundamentals of Crash Sensing in Automotive Air Bag Systems*. Published by SAE International. 2000.
3. Hadrys, D. & Kubik, A. & Stanik, Z. Deceleration and deformation during dynamic loading of model car body parts after post-accident repair. *Transport Problems*. 2020. Vol. 15 No. 3. P. 5-16.
4. Hadrys, D. & Kubik, A. & Stanik, Z. Deceleration and deformation during dynamic load of model longitudinals - real conditions and simulation. *Scientific Journal of Silesian University of Technology. Series Transport*. 2019. Vol. 102. P. 53-64.

5. Hannan, M.A. & Hussai, A. & Mohamed, A. & Samad, S.A. & Wahab, D.A. Decision fusion of a multi-sensing embedded system for Occupant safety measures. *International Journal of Automotive Technology*. 2010. Vol. 11. No. 1. P. 57-65.
6. Heidrich, S. *Innovative-Längsträgerinstandsetzung*. Germany, Lohfelden: Kraftfahrzeugtechnisches Institut, 2010. [In German: *Innovative Longitudinal Beam Repair*].
7. Heidrich, S. *Reparaturuntersuchung*. Germany, Lohfelden: Kraftfahrzeugtechnisches Institut, 2007. [In German: *Repair Inspection*. Germany, Lohfelden: Automotive Engineering Institute].
8. International Motor Vehicle Inspection Committee Report 8328. *A Test Procedure for Airbags*. Institut für Kraftfahrwesen Aachen. 2000.
9. Jia, Q. & Guo, W. & Li, W. Experimental and numerical study on local mechanical properties and failure analysis of laser welded DP980 steels. *Materials Science and Engineering*. 2017. Vol. 680. P. 378-387.
10. Kaczyński, P. & Rusiński, E. *Ocena wytrzymałości połączeń punktowych w cienkościennych strukturach energochłonnych*. Wrocław: Oficyna Wydawnicza Politechniki Wrocławskiej. 2014. [In Polish: *Evaluation of the Strength of Spot Connections in Thin-Walled Energy-Absorbing Structures*. Wrocław: Publishing House of Wrocław University of Science and Technology].
11. Kamiński, T. & Niezgodna, M. & Kruszewski, M. Collision detection algorithms in the ecall system. *Journal of KONES Powertrain and Transport*. 2012. Vol. 19 No. 4. P. 267-274.
12. Lee, J.K. & Ha, W. & Lee, J.H. & Chae, D.B. & Kim, J.H. Validation methodology on airbag deployment process of driver side airbag. *Computer Science*. 2009. ID: 86543525.
13. Majlinger, K. & Kalacska, E. & Spena, P.R. Gas metal arc welding of dissimilar AHSS sheets. *Materials & Design*. 2016. Vol. 109. P. 615-621.
14. *NHTSA VSR - NHTSA Vehicle Crash Test Database*. Available at: <https://www-nrd.nhtsa.dot.gov/database/veh/veh.htm> (No. crashtest: TC 03-228 RR04-232, Tc 03-229 RR04-221, DTS-TRC-03-005, 030806-1, 060502-1, NCAP-MGA-2001-004).
15. Park, G. & Bae, G. & Lee, Ch. Characterization of mechanical and metallurgical notch effects of DP980 steel weld joints in fatigue performance. *Metallurgical and Materials Transactions A*. 2019. Vol. 50. No. 3. P. 1294-1307.
16. Rastegar, V. & Marzbanrad, J. Modeling and simulation of vehicle airbag behaviour in crash. *International Scientific Journal "Industry 4.0"*. 2018. Vol. 3. P. 126-129.
17. Stephen, T. & Gere, J. *Teoria stateczności sprężystej*. Warszawa: Arkady, 1963. [In Polish: *Elastic Stability Theory*. Warsaw: Arkady, 1963].
18. *Transportation of department. Federal Motor Vehicle Safety Standards; Occupant Crash Protection.: National Highway Traffic Safety Administration*. FMVSS No. 208. P. 552, 571, 585, 595. Available at: <https://www.nhtsa.gov/laws-regulations>.
19. Wang, J. & Yang, L. Effect of energy input on the microstructure and properties of butt joints in DP1000 steel laser welding. *Materials & Design*. 2016. Vol. 90. P. 642-649.
20. Wang, X. & Sun, Q. & Zheng, Z. Microstructure and fracture behavior of laser welded joints of DP steels with different heat inputs. *Materials Science and Engineering*. 2017. Vol. 699. P. 18-25.
21. Wang, X. & Luo, Z. & Liu, Y. & Ling F. Fatigue properties of advanced high strength steel plate welded by hybrid plasma arc welding. *Procedia Structural Integrity*. 2019. Vol. 22. P. 59-63.
22. Winch, M.J. & Hollowell, T.W. & Kianianthra, J. & Evans, W.D. *Air Bag Technology in light passenger vehicles*. USA: Office of Research and Development National Highway Traffic Safety Administration, 2001.
23. Vangi, D. *Vehicle Collision Dynamics, Analysis and Reconstruction*. Florence, Italy: Department of Industrial Engineering. University of Florence. 2020.